CHEMISTRY

A single-stranded coordination copolymer affords heterostructure observation and photoluminescence intensification

Ryojun Toyoda[1], Ryota Sakamoto[1,2]*, Naoya Fukui[1], Ryota Matsuoka[1], Mizuho Tsuchiya[1], Hiroshi Nishihara[1]

Few artificial systems can be exfoliated into, and observed as, single wires with lengths of more than several micrometers, and no previous example features a copolymer structure; this is in contrast with biopolymers such as single-strand DNAs. Here, we create a set of one-dimensional coordination copolymers featuring bis(dipyrrinato)zinc complex motifs in the main chain. A series of random copolymers is synthesized from two types of bridging dipyrrin proligand and zinc acetate, with various molar ratios between the proligands. Sonication of the bulk solid copolymer in organic solvent exfoliates single strands with lengths of 1.4 to 3.0 μm. Atomic force microscopy at ambient conditions visualizes the copolymer structure as height distributions. The copolymer structure improves its photoluminescence (up to 32%) relative to that of the corresponding homopolymers (3 and 10%). Numerical simulation based on a restricted random walk model reproduces the photoluminescence intensification, suggesting at the same time the existence of fast intrawire exciton hopping.

INTRODUCTION

Heterostructures in polymers (or copolymer configurations) enrich their functionalities, and numerous works have studied organic polymers that feature random (*1*–*4*), block (*5*–*14*), and sequence-controlled (*15*–*21*) copolymer compositions. For example, Roy *et al.* (*14*) reported a fundamental intramolecular charge-transfer mechanism for donor-π-acceptor copolymers, which led to the fabrication of energy-efficient organic solar cells. Researchers have also developed supramolecular copolymers based on noncovalent bonds such as hydrogen bonds, metal coordination bonds, and π-π interactions (*22*–*30*).

One of the ultimate goals in polymer science is to use single fibers like natural systems use one-dimensional (1D) copolymers, e.g., DNAs, whose base sequences designate the primary structures of proteins. In contrast, single strands of 1D artificial polymers have not yet been developed for useful applications; very recently, Gómez-Herrero and Zamora have performed a conductivity measurement for a single MMX chain (*31*). An obstacle lies in the difficulty of exfoliating them into, and isolating them as, single strands. Associated with this, single-strand artificial polymers have rarely been observed at ambient conditions (*32*–*34*), and none has had its heterostructure visualized. In contrast, natural polymers (e.g., the sequences of single-stranded DNA) have been deciphered by scanning tunnel microscopy (*35*–*37*). In this context, we have recently reported on 1D coordination homopolymers featuring the bis(dipyrrinato)zinc(II) complex motif (e.g., Homo-1 in Fig. 1A) (*38*, *39*). The series of coordination polymers can be exfoliated into single strands upon sonication in organic media. In addition, by sampling a dispersion of the homopolymer on a flat substrate like highly ordered pyrolytic graphite (HOPG), single strands can be observed by atomic force microscopy (AFM). Their functionality has been demonstrated to include thermoelectric conversion (upon conjugation with single-walled carbon nanotubes), photoelectric conversion, and circularly polarized luminescence (by the introduction of a chiroptical structure).

In this work, we create sets of bis(dipyrrinato)zinc(II) coordination copolymers, Co-1-*k* and Co-2-*k* (Fig. 1B). The rigid and steric skeleton of the copolymer allows it to be exfoliated into single strands. Taking advantage of the chemical and steric structural features of the copolymer, here, we focus on the following three distinctive aspects. (i) This work offers the first attempt to observe the heterostructure of artificial 1D copolymers using AFM at ambient conditions. (ii) The generally poor photoluminescence (PL) ability of the bis(dipyrrinato)zinc(II) homopolymers (e.g., 3 and 10% PL quantum yields of Homo-1 and Homo-3, vide infra) is enhanced by our strategy originally applied to dipyrrinato-metal complex small molecules (*40*–*45*). (iii) A simple numerical simulation based on a restricted random walk is used to elucidate the PL enhancement and to imply the existence of fast intrawire exciton migration.

RESULTS

Preparation of the coordination copolymers

Figure 1B outlines the synthesis of coordination copolymers Co-1-*k* and Co-2-*k*. The strategy is simple: Two different bridging dipyrrin proligands (H_2L1 and H_2L3 for Co-1-*k*; H_2L2 and H_2L3 for Co-2-*k*) are mixed with zinc acetate in dichloromethane/methanol (2:1, v/v) and stored still for several days at room temperature. The chelation between the dipyrrin proligand and zinc(II) ion proceeds spontaneously without additional base (*46*, *47*) and forms the random copolymer as precipitate. H_2L3 comprises plain dipyrrin, whereas H_2L1 and H_2L2 have arylethynyl groups at the β position of the dipyrrin moiety; this modification affords π-expansion, leading to narrower HOMO-LUMO gaps and smaller photoexcitation energies. Note that proligand H_2L3 and its close analog H_2L3′ were further identified by single-crystal x-ray structure analysis as HBr salts (fig. S1 and table S1). Seven samples of Co-1-*k* (*k* = 1 to 7) were prepared by changing *r*, the mixing ratio of proligand H_2L1 to (H_2L1 + H_2L3) (Fig. 1C); a greater *k* indicates a higher proportion of H_2L1. The actual ratio of bridging ligand L1 to (L1 + L3) incorporated in Co-1-*k* (defined as *x*, Fig. 1C) is described later. The Co-1-*k* series enables us to study the effect of copolymer composition on the photophysical properties and single wire observation. In a similar

[1]Department of Chemistry, Graduate School of Science, The University of Tokyo, 7-3-1 Hongo, Bunkyo-ku, Tokyo 113-0033, Japan. [2]JST-PRESTO, 4-1-8 Honcho, Kawaguchi, Saitama 332-0012, Japan.
*Corresponding author. Email: sakamoto@chem.s.u-tokyo.ac.jp.

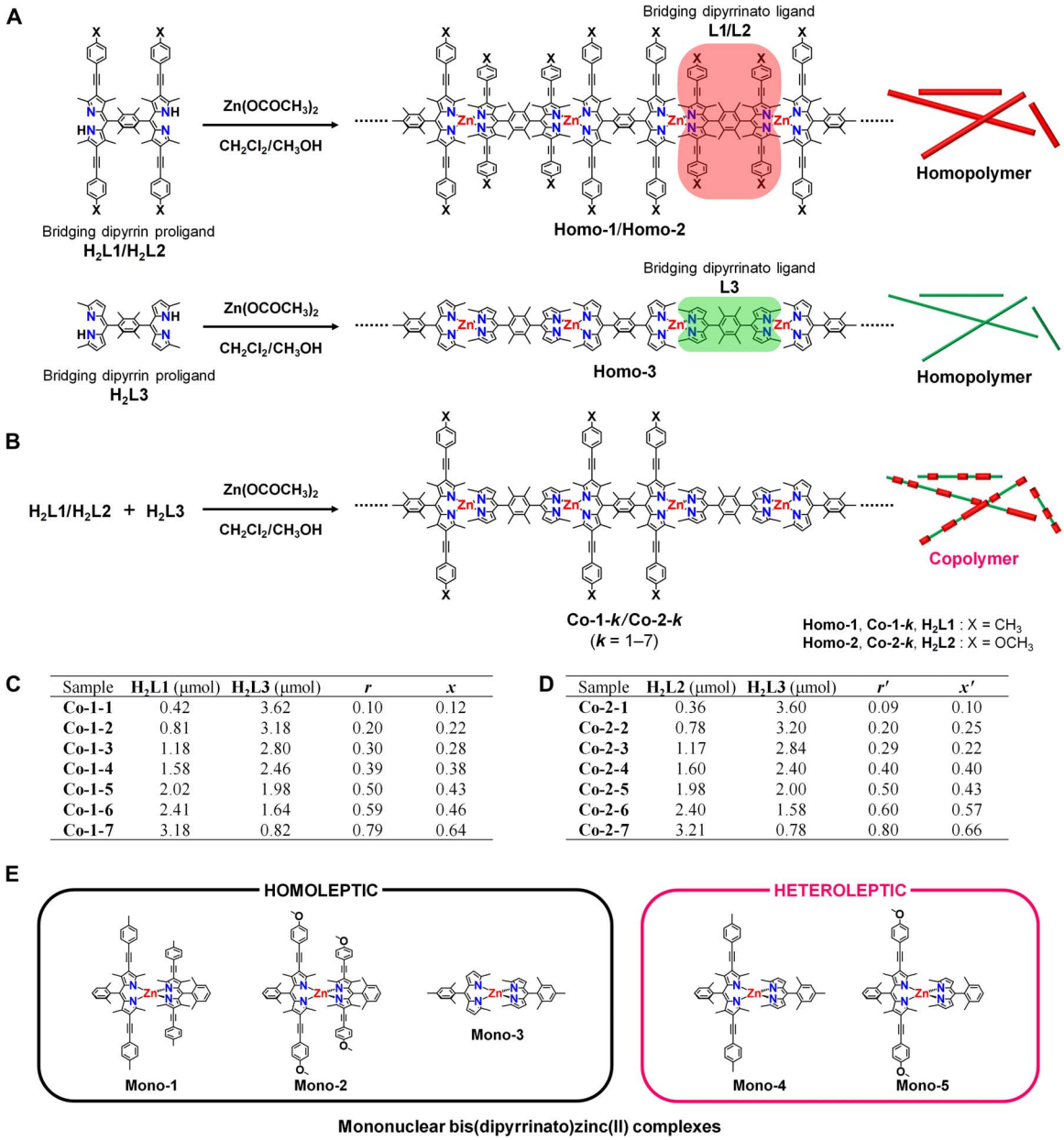

C

Sample	H_2L1 (μmol)	H_2L3 (μmol)	r	x
Co-1-1	0.42	3.62	0.10	0.12
Co-1-2	0.81	3.18	0.20	0.22
Co-1-3	1.18	2.80	0.30	0.28
Co-1-4	1.58	2.46	0.39	0.38
Co-1-5	2.02	1.98	0.50	0.43
Co-1-6	2.41	1.64	0.59	0.46
Co-1-7	3.18	0.82	0.79	0.64

D

Sample	H_2L2 (μmol)	H_2L3 (μmol)	r'	x'
Co-2-1	0.36	3.60	0.09	0.10
Co-2-2	0.78	3.20	0.20	0.25
Co-2-3	1.17	2.84	0.29	0.22
Co-2-4	1.60	2.40	0.40	0.40
Co-2-5	1.98	2.00	0.50	0.43
Co-2-6	2.40	1.58	0.60	0.57
Co-2-7	3.21	0.78	0.80	0.66

Fig. 1. Bis(dipyrrinato)zinc(II) coordination polymers and mononuclear complexes. (**A** and **B**) Synthetic schemes and chemical structures of (A) homopolymers Homo-1 to Homo-3 and (B) copolymers Co-1-*k* and Co-2-*k* (*k* = 1 to 7). Chemical structures of constitutive bridging dipyrrin proligands (H_2L1, H_2L2, and H_2L3) and bridging dipyrrin ligands (L1, L2, and L3) are also provided. (**C**) Moles of proligands H_2L1 and H_2L3 used to prepare Co-1-*k* are listed. *r* and *x* denote the mixing ratio of H_2L1 to (H_2L1 + H_2L3) and actual mole fraction of L1 in Co-1-*k*, respectively. (**D**) Moles of proligands H_2L2 and H_2L3 used to prepare Co-2-*k* are listed. *r*′ and *x*′ denote the mixing ratio of H_2L2 to (H_2L2 + H_2L3) and actual mole fraction of L2 in Co-2-*k*, respectively. (**E**) Chemical structures of mononuclear complexes Mono-1 to Mono-5. The heteroleptic complexes (Mono-4 and Mono-5) show brighter fluorescence than the homoleptic ones (Mono-1 to Mono-3).

manner, Co-2-*k* samples were prepared (*k* = 1 to 7, with compositional parameters *r*′ and *x*′; Fig. 1D). Corresponding homopolymers Homo-1, Homo-2, and Homo-3 (Fig. 1A) were also prepared as references in accordance with our previous report (*38*).

X-ray photoelectron spectroscopy

The resultant coordination polymers, together with the starting bridging dipyrrin proligands, were analyzed using x-ray photoelectron spectroscopy (XPS) (fig. S2). Proligands H_2L1 (397.4 and 398.8 eV), H_2L2 (398.1 and 399.7 eV), and H_2L3 (397.8 and 399.5 eV) show two peaks in the N 1s spectral region (fig. S2, A to C). The peak located at lower binding energy stems from iminic nitrogen of the dipyrrin part, whereas that at higher binding energy is derived from pyrrolic nitrogen (*38*, *39*). In contrast, coordination polymers Homo-1, Homo-2, Homo-3, Co-1-7, and Co-2-7 show a single peak for N 1s at 397.8 to 398.5 eV, which originates from the homogenization of the two chemically different nitrogen atoms upon deprotonation and coordination to the zinc center (fig. S2, D to H). The coordination polymers showed

an additional peak in the Zn $2p_{3/2}$ region at 1020.6 to 1021.7 eV, whereas the proligands lacked such a peak. Nitrogen-to-zinc ratios for the coordination polymers were calculated from the peak areas corrected by photoionization cross-section, giving N:Zn values of 20.6:79.4 (Homo-1), 20.9:79.1 (Homo-2), 21.7:78.3 (Homo-3), 20.9:79.1 (Co-1-7), and 21.0:79.0 (Co-2-7) (fig. S3). The values are consistent with the ideal value of 1:4 (= Zn/N ratio of 0.25) for the bis(dipyrrinato)zinc(II) complex motif. Figure S4 shows the elemental abundance for the Co-1-*k* series and Homo-1 determined by elemental analysis and inductively coupled plasma atomic emission spectrometry (ICP-AES). Notably, the Zn/N ratio is plotted in fig. S4E, which shows consistency with the theoretical value and XPS result. The series of elemental abundance analyses indicates the formation of the desired coordination polymers.

Strategy for PL enhancement

We previously reported the enhancement of PL in mononuclear dipyrrinato-metal complexes (*40*–*45*). When the two dipyrrinato ligands that coordinate to the zinc center are identical (e.g., homoleptic complexes Mono-1, Mono-2, and Mono-3; Fig. 1E), the complexes show only slight fluorescence because of interligand charge separation and subsequent nonradiative deactivation to the ground state (fig. S5A) (*44*). On the other hand, when the zinc ion binds to two different ligands (e.g., heteroleptic complexes Mono-4 and Mono-5; Fig. 1E), interligand charge separation is suppressed by appropriate frontier orbital ordering and much brighter PL is induced (fig. S5B). We expect that this strategy is valid even for 1D coordination polymers and may compensate the poor PL properties of homopolymers (e.g., the 3% PL quantum yield of Homo-1, vide infra) by fabricating corresponding copolymers that contain heteroleptic complex motifs. This strategy works well, however, intrawire exciton migration is also required to elucidate the PL intensification (discussed in the later section).

Exfoliation into single wires

The Zn center adopts a tetrahedral coordination sphere, and consequently, the wire skeleton has a nonplanar steric structure (*38*). This structural feature should deteriorate interstrand attractive forces, facilitating single-wire exfoliation. Sonication (25°C, 360 W, 38 kHz, 30 min; Fig. 2A) of the coordination copolymer separated as solid in an organic solvent like toluene can exfoliate it into single strands. A dispersion of Co-1-3 in toluene showed Tyndall scattering upon illumination with a red laser flux (Fig. 2B), implying the existence of a molecular superstructure with a size of at least several hundred nanometers. On the other hand, when a green laser flux was applied, Tyndall scattering was concealed with an orange luminous streak (Fig. 2C), which was derived from the PL of Co-1-3 (vide infra), allowing us to anticipate the PL intensification.

Composition of the copolymers

The ultraviolet/visible (UV/vis) spectra of solutions of bridging dipyrrin proligands H_2L1 and H_2L3 and dispersions of homopolymers Homo-1 and Homo-3 in toluene are overlaid in Fig. 2D. The absorption maxima of H_2L1 and H_2L3 (at 505 and 436 nm, respectively) are ascribable to the $^1\pi$-π^* transition of the dipyrrin moiety (*38*). The red shift shown by H_2L1 relative to H_2L3 derives from π-expansion by the (4-methylphenyl)ethynyl group. The $^1\pi$-π^* bands of Homo-1 and Homo-3 are shifted bathochromically relative to those of H_2L1 and H_2L3 and feature maxima at 550 and 490 nm. This series of spectral changes is typical of the formation of the bis(dipyrrinato)zinc(II) complex motif (*40*). The spectrum of Co-1-*k* features two peaks at 550 and 490 nm (Fig. 2E), which are consistent with the $^1\pi$-π^* bands of Homo-1 and Homo-3, thereby verifying the copolymer composition. The spectra in Fig. 2E are normalized at 490 nm, which shows that the contribution from L1 increases as the mixing ratio of H_2L1 to (H_2L1 + H_2L3) (*r*; Fig. 1C) increases. The actual mole fraction (*x*) of L1 to (L1 + L3) in Co-1-*k* was estimated from the relative intensity of the two absorption peaks and was proportional to *r* (Figs. 1 and 2F). Hence, the composition of the coordination copolymer is tunable by the mixing ratio *r*. The slope of the plot (0.84) is less than unity, which reflects the weaker coordination ability of L1 relative to L3 due to the electron-withdrawing (4-methylphenyl)ethynyl group in L1. Similar spectra

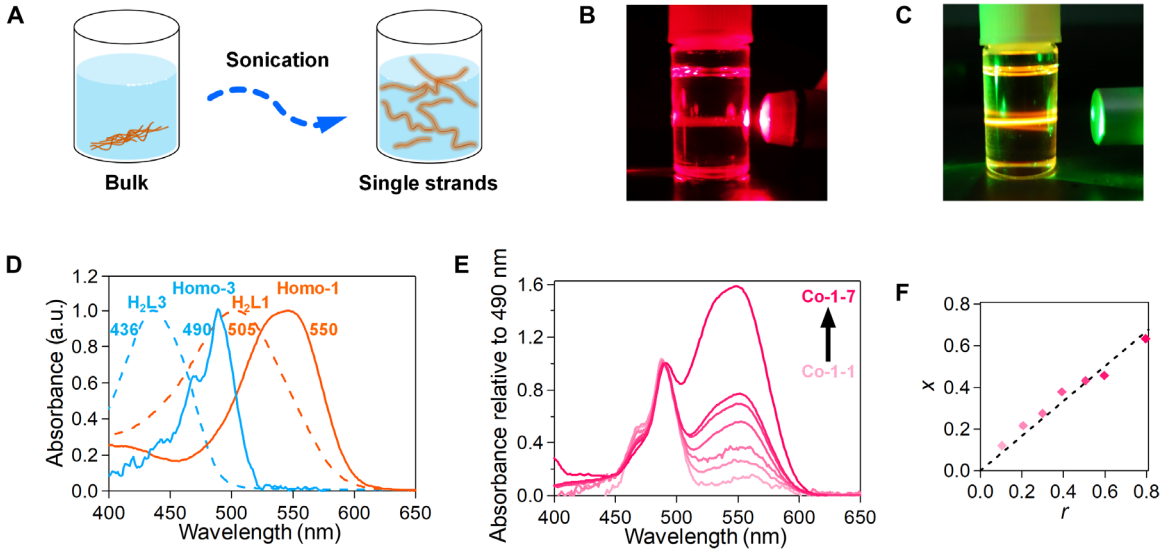

Fig. 2. Exfoliation and UV/vis spectroscopy in toluene. (**A**) Exfoliation of the coordination polymer into single strands. (**B** and **C**) Photographs of a toluene dispersion of Co-1-3 upon illumination with laser flux: (B) red and (C) green. In (C), the green flux scattering is concealed with orange PL. (**D**) Normalized UV/vis spectra of bridging dipyrrin proligands H_2L1 and H_2L3 and homopolymers Homo-1 and Homo-3. a.u., arbitrary units. (**E**) UV/vis spectra of Co-1-*k* (*k* = 1 to 7) normalized at 490 nm. (**F**) Relationship between the actual mole fraction of L1 to (L1 + L3) in Co-1-*k* (*x*) and mixing ratio of H_2L1 to (H_2L1 + H_2L3) (*r*).

and discussion are available for Co-2-*k* (Fig. 1 and fig. S6). The plot for Co-2-*k* shows a greater slope (0.97) for the relationship between x' and r' than for Co-1-*k*; this stems from the electron-donating ability of the methoxy group over the methyl group, which compensates the degradation of the coordination ability of the π-expanded dipyrrinate moiety in L2.

Photoelectric conversion

We previously reported the photoelectric conversion ability of the homopolymers that takes advantage of its intense visible light absorptivity (*38*). Given that the copolymer has a broader absorption spectrum (Fig. 2E) than the corresponding homopolymers, it is expected to produce a broader photoresponse than the homopolymers. A SnO_2 substrate modified with Co-1-6 (fig. S7A) served as a photoanode in a three-electrode system (fig. S8). Irradiation induced anodic photocurrent to flow through the system (fig. S7B). The action spectrum of the photocurrent generation for Co-1-6 covers a broader wavelength range (450 to 600 nm) than that of either Homo-1 or Homo-3 (fig. S7, C to E).

AFM evidence of the copolymer structure

The bidentate coordination of the dipyrrinato ligand and orthogonally fixed dihedral angles among the dipyrrinato and durene units (*38*) should allow the coordination copolymer to bear a rigid framework. Together with the single-wire exfoliation described in the previous section, we attempted to observe the copolymer structure of Co-1-*k* using AFM at ambient conditions; to the best of our knowledge, this is the first AFM study of artificial polymer single strands. A dispersion of Co-1-3 was dropcast onto HOPG with a hydrophobic surface, which then underwent AFM analysis. The representative AFM height image in Fig. 3A shows several molecular wires (with lengths of 1.4 to 3.0 μm) as slightly winding white streaks. The zinc-zinc distance quantified by single-crystal x-ray structure analysis for a bis(dipyrrinato) zinc(II) coordination homopolymer (1.26 nm) (*38*) indicates that Co-1-3 comprises 1100 to 2400 mers. Note that exfoliated Co-1-3 was also observed on MoS_2 with a hydrophobic surface, while hydrophilic SiO_2/Si and mica did not give one (fig. S9). Height data collected for each strand are summarized in the height histograms in Fig. 3B, which show that the average heights converged in a narrow range (1.21 to 1.42 nm), confirming the uniformity of the exfoliated molecular wires. Figure 3C shows a combined height histogram for Co-1-3 that assembles all height values of each nanowire; similarly analyzed data for Homo-1 and Homo-3′ (a close analog of Homo-3; fig. S11A) are also overlaid (figs. S10 and S11). Figure 3C indicates that Co-1-3 has an average height (1.30 ± 0.01 nm) intermediate between those of Homo-1 and Homo-3′ (1.94 ± 0.01 nm and 0.74 ± 0.01 nm, respectively). Note that the average heights of Homo-1 and Homo-3′ are consistent with the size of corresponding mononuclear bis(dipyrrinato)zinc(II) complexes Mono-1 (1.81 nm) and Mono-3′ (0.65 nm) (Fig. 3D). The slight inconsistency likely arose from van der Waals contacts between the HOPG substrate surface and the nanowire and between the AFM tip and the nanowire (an AFM tip is far greater than the molecular scale). The heights measured here by AFM should reflect the "average" height of the molecular wire, thus accounting for the observed intermediate height values for copolymer Co-1-3. Therefore, this AFM analysis supports that the white streaks in Fig. 3A are single wires of copolymer Co-1-3. Single strands of Co-1-1, Co-1-2, Co-1-5, and Co-1-7 were also similarly analyzed by AFM (Fig. 3, E, G, I, and K), and like Co-1-3, their heights were intermediate between those of the corresponding homopolymers (Fig. 3, F, H, J, and L). The height histograms of Co-1-*k* were fitted with Gaussian functions (fig. S12), and the resulting curves are shown together in Fig. 3M. Figure 3N plots the Gaussian peak positions of the coordination homo- and copolymers (H_{gauss}) and the actual mole fraction of the bulky bridging dipyrrinato ligand L1 (x), showing that the height of the molecular wire increases as x increases. This further supports the copolymer structure of Co-1-*k*.

PL spectroscopy

Figure 4A shows fluorescence spectra of exfoliated Homo-1 and Homo-3 as toluene suspensions. The molecular wires were illuminated with 550 and 490 nm light, respectively, which photoexcited their ^{1}π-π* bands. Homo-1 and Homo-3 showed luminescence at 600 and 512 nm, respectively, which are assignable to the ^{1}π-π* emissions of the π-expanded and plain dipyrrinato ligands, L1 and L3, respectively (*43*). Figure 4 (B to H) depicts the spectra of exfoliated Co-1-*k* (k = 1 to 7). Illumination with 550-nm light selectively stimulated π-expanded dipyrrinato ligand L1, causing Co-1-*k* to emit exclusively at 600 nm. This luminescence stems from L1, in comparison to that of Homo-1. Characteristic features appeared upon illumination with 490-nm light, which chiefly photoexcites the plain dipyrrinato ligand L3. Copolymers Co-1-*k* (k = 1 to 3) showed dual emission at 600 and 512 nm, but the relative intensity of the luminescence at 512 nm (derived from ligand L3) decreased significantly as k increased. Copolymers Co-1-*k* (k = 4 to 7) emitted exclusively at 600 nm (from ligand L1), with no emission peak at 512 nm. These results indicate that energy transfer from L3 to L1 occurred in copolymers Co-1-*k*.

Spectroscopic evidence of the copolymer structure

The energy transfer described in the previous section provides evidence of the copolymer structure. Corroboration came through UV/vis and fluorescence spectroscopy of a mixture of exfoliated homopolymers Homo-1 and Homo-3 in toluene (Homo-1 + Homo-3). The spectra in Fig. 4 (I and J) are overlaid with those of Co-1-4. The UV/vis spectra show that the proportion of ligand L1 is greater in Homo-1 + Homo-3 than in Co-1-4, as the relative intensity of the 490-nm absorption is higher in Homo-1 + Homo-3. Nonetheless, excitation with 490-nm light caused Homo-1 + Homo-3 to emit at 512 nm from ligand L3, with negligible luminescence at 600 nm from ligand L1. This result is in complete contrast with the exclusive 600-nm emission from Co-1-4. This comparative experiment demonstrates that intrawire energy transfer is far more efficient than interwire transfer (Fig. 4K), thereby indicating that Co-1-4 forms a copolymer incorporating both L1 and L3 rather than a mixture of the corresponding homopolymers.

PL enhancement

The quantum yields (ϕ_{PL}) and lifetimes (τ_{PL}) of the PL of exfoliated copolymers Co-1-*k* are listed in table S2, together with those of the corresponding homopolymers Homo-1 and Homo-3. ϕ_{PL} is also plotted against x in Fig. 5 with those from additional copolymer samples. Each sample was excited at either 550 nm (Fig. 5A) or 490 nm (Fig. 5B). Under excitation at 550 nm, Co-1-*k* shows a monotonic increase in ϕ_{PL} as the actual mole fraction of L1 (x) becomes smaller. This tendency is consistent with the τ_{PL}-x plot (fig. S13). As a result, Co-1-1 (x = 0.12) achieved the highest ϕ_{PL} value of 0.32, which is much greater than that of the corresponding homopolymer Homo-1 (ϕ_{PL} = 0.03). The ϕ_{PL}-x plot measured under excitation at 490 nm forms a bell curve, with Co-1-3 (x = 0.28) showing the highest ϕ_{PL} of 0.25, which is

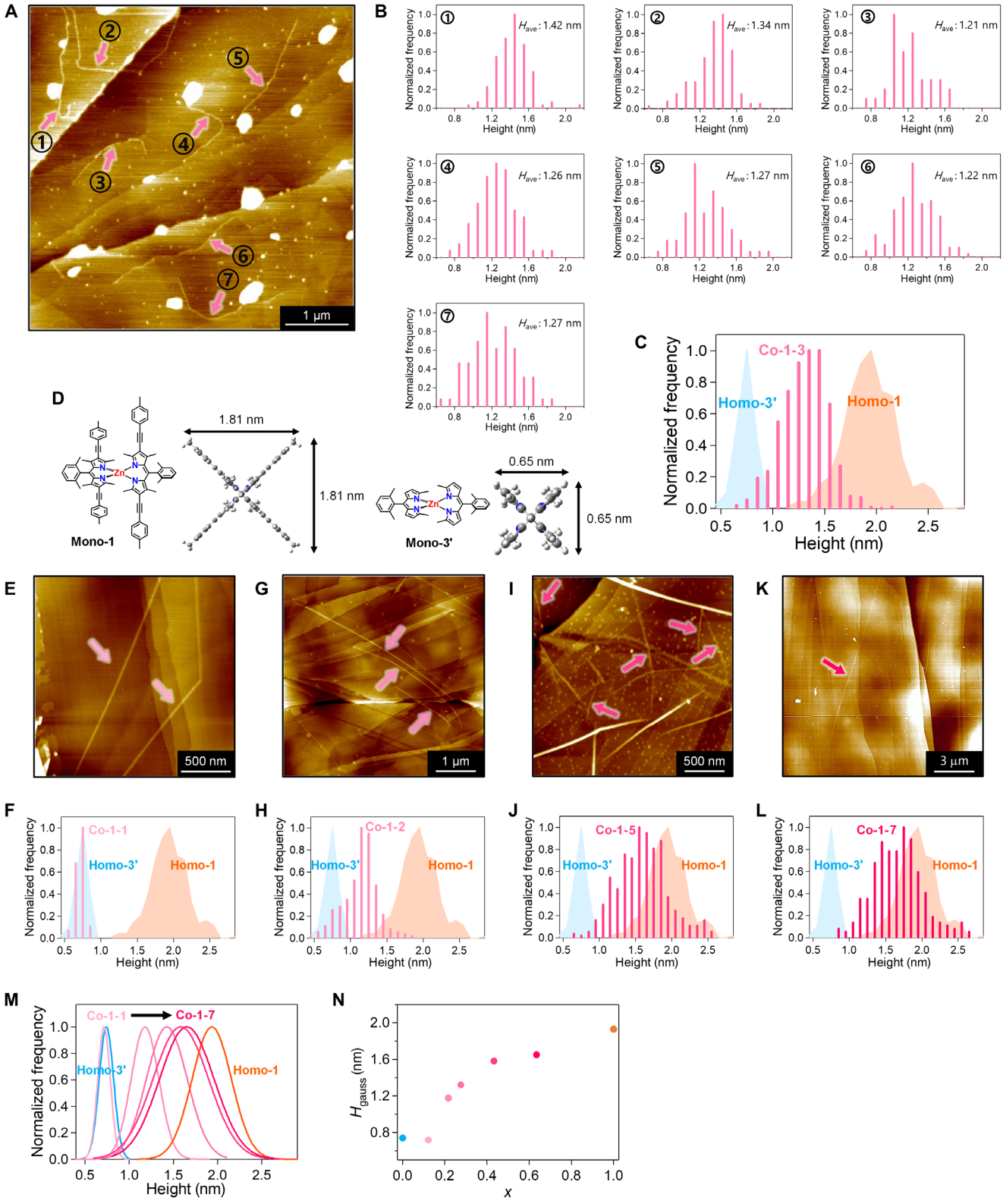

Fig. 3. AFM analysis. (**A**) AFM height image of single strands of Co-1-3 appearing as white lines on a HOPG substrate. (**B**) Height histograms for individual single strands of Co-1-3. (**C**) Height histograms for all single strands of Co-1-3 (magenta), Homo-1 (orange shaded), and Homo-3′ (blue shaded). (**D**) Chemical structures of corresponding mononuclear complexes Mono-1 and Mono-3′, with sizes estimated by density functional theory (DFT) calculation. AFM images of (**E**) Co-1-1, (**G**) Co-1-2, (**I**) Co-1-5, and (**K**) Co-1-7. Height histograms for (**F**) Co-1-1, (**H**) Co-1-2, (**J**) Co-1-5, and (**L**) Co-1-7, along with those of Homo-1 (orange shaded) and Homo-3′ (blue shaded). (**M**) Gaussian-fitted height histograms for Co-1-*k*, Homo-1, and Homo-3′. (**N**) Plot of central value of Gaussian curve and actual mole fraction of L1 (*x*) for Co-1-*k*, Homo-1, and Homo-3′.

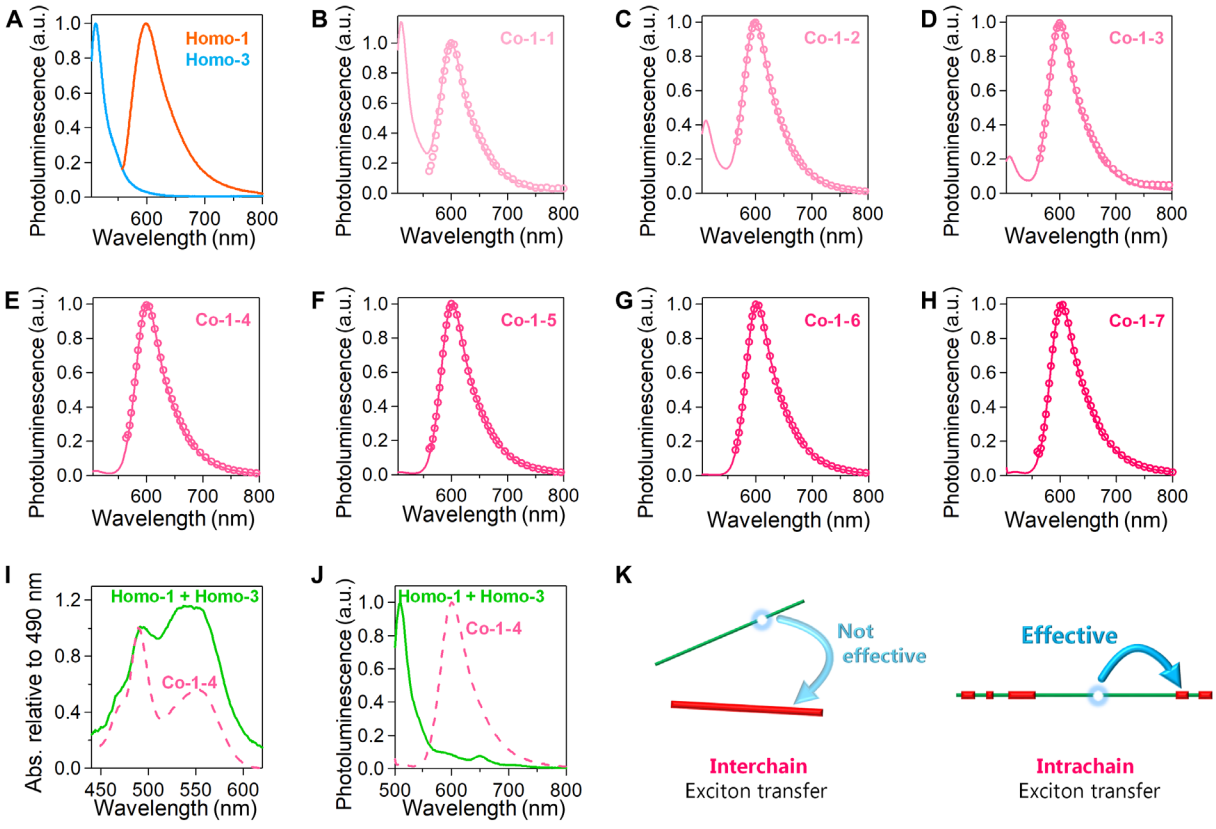

Fig. 4. PL spectroscopy in toluene. (**A**) PL spectra of Homo-1 (magenta) and Homo-3 (green) excited at 550 and 490 nm, respectively. (**B** to **H**) Co-1-*k* (*k* = 1 to 7) excited at 550 nm (circles) and 490 nm (solid lines). (**I**) UV/vis spectra of Homo-1 + Homo-3 (solid line) and Co-1-4 (dotted line) with normalization at 490 nm. (**J**) PL spectra of Homo-1 + Homo-3 (solid line) and Co-1-4 (dotted line) upon excitation with 490-nm light. (**K**) Illustration of exciton transfer behavior: interwire exciton transfer in Homo-1 + Homo-3 is negligible, whereas intrawire exciton transfer in Co-1-4 is efficient.

greater than that of Homo-1 and that of Homo-3 (ϕ_{PL} = 0.10). Similar experiments were conducted for Co-2-*k* in toluene (figs. S14 and S15). The luminescence from ligand L2 (613 nm in toluene) shifted bathochromically relative to that of L1 (600 nm) because of the electron-donating ability of the methoxy groups. The PL analysis again revealed a trend similar to that seen in Co-1-*k*. The maximal ϕ_{PL} reached 0.25 in toluene, which is greater than those of Homo-2 (ϕ_{PL} = 0.03) and Homo-3 (ϕ_{PL} = 0.10).

Numerical simulation for the PL property

As demonstrated by the study of intrawire and interwire energy transfer (Fig. 4, I to K) and AFM analysis (Fig. 3), samples Co-1-*k* certainly have a copolymer structure. The dipyrrinato ligand units incorporated in the copolymer are classified into four species (Fig. 6A): $D_{Homo\text{-}L1}$ and $D_{Homo\text{-}L3}$ from the homoleptic complex moiety, and $D_{Hetero\text{-}L1}$ and $D_{Hetero\text{-}L3}$ from the heteroleptic complex moiety. The proportion of each of the four dipyrrinato units is determined by the ratio of ligand L1 to (L1 + L3) (*x*) following Eqs. 1 to 3 when the wire is long enough to ignore the terminus

$$P(D_{Homo\text{-}L1}) = x^2 \quad (1)$$

$$P(D_{Homo\text{-}L3}) = (1-x)^2 \quad (2)$$

$$P(D_{Hetero\text{-}L1}) = P(D_{Hetero\text{-}L3}) = x(1-x) \quad (3)$$

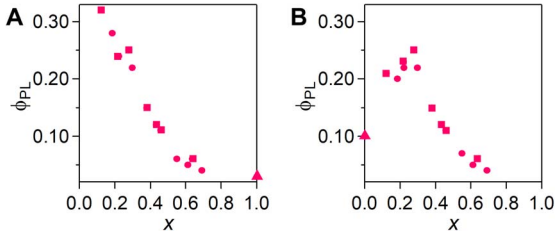

Fig. 5. PL quantum yield dependence on *x* in toluene. (**A** and **B**) φ_{PL}-*x* plots for coordination copolymers Co-1-*k* (*k* = 1 to 7, squares), homopolymers (Homo-1 and Homo-3, triangles), and additional copolymer samples (circles) excited at (A) 550 nm and (B) 490 nm.

where $P(D_{Homo\text{-}L1})$, $P(D_{Homo\text{-}L3})$, $P(D_{Hetero\text{-}L1})$, and $P(D_{Hetero\text{-}L3})$ are the proportions of $D_{Homo\text{-}L1}$, $D_{Homo\text{-}L3}$, $D_{Hetero\text{-}L1}$, and $D_{Hetero\text{-}L3}$, respectively. Figure S16 shows plots of ϕ_{PL} with respect to *x* assuming that an exciton is generated at one of the dipyrrinate sites in accordance with the excitation wavelength and the probabilities given by Eqs. 1 to 3, and that intrawire exciton hopping is not valid. However, it does not reproduce the characteristic bell curve for excitation at 490 nm. We regard the discrepancy as the consequence of intrawire exciton migration, thereby conducting numerical simulation that takes the migration into consideration (Fig. 6B). A virtual Co-1-*k* strand was constructed by placing 1000 molecules of L1 and L3 randomly (corresponding to a 1.26-μm-long wire), with their abundance ratio

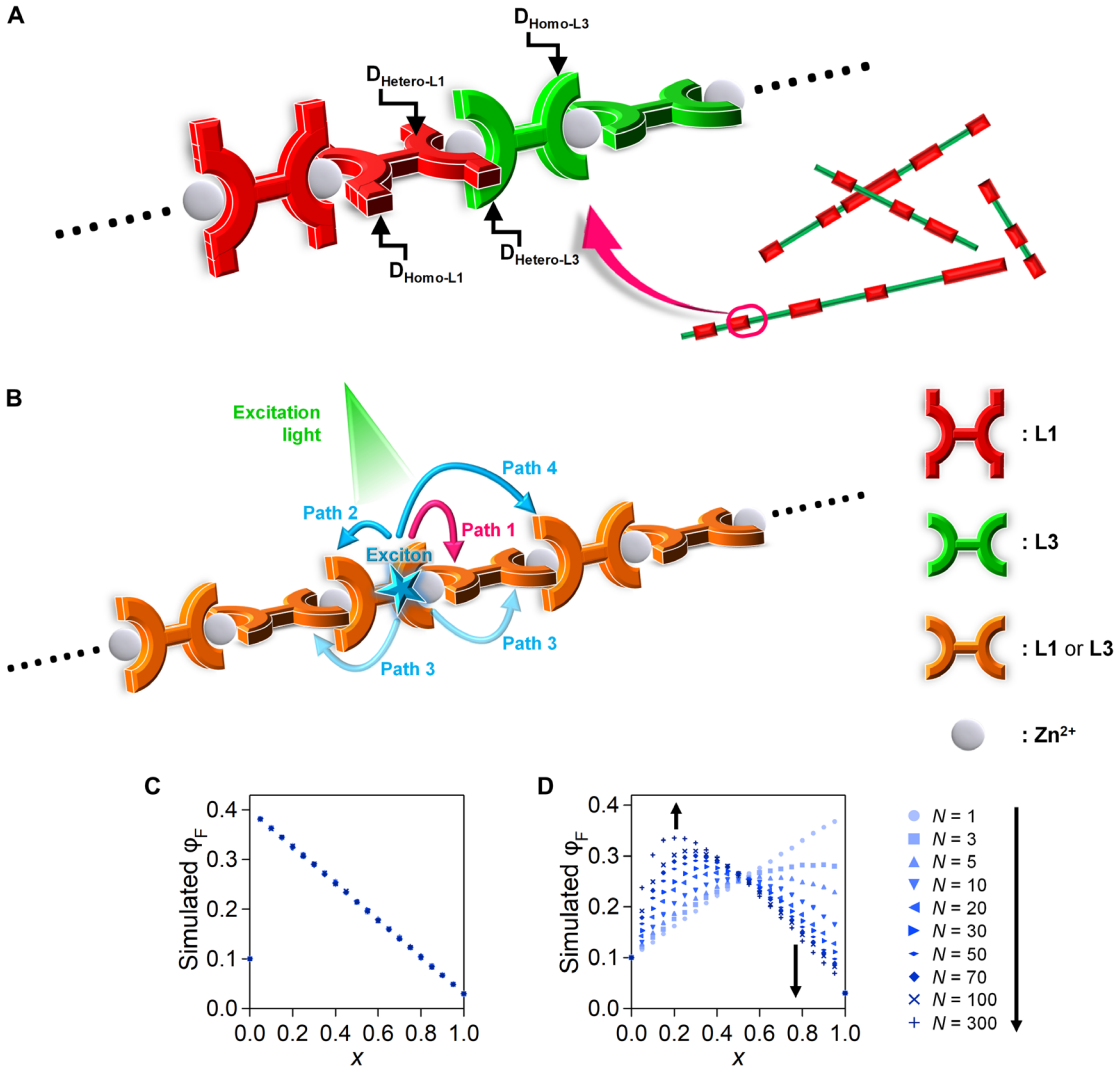

Fig. 6. Numerical simulation for PL efficiency. (**A**) Four types of constituent dipyrrinato ligands in coordination copolymers Co-1-*k*, $D_{Homo-L1}$, $D_{Homo-L3}$, $D_{Hetero-L1}$, and $D_{Hetero-L3}$. (**B**) Possible intrawire exciton migration pathways considered in the numerical simulation. (**C** and **D**) Simulated φ_{PL}-*x* plot with various *N* when excited at (C) 550 nm and (D) 490 nm.

set according to the experimental *x* value. A modified 1D random walk model is considered for the intrawire exciton migration, the details of which are described in (i) to (iii) below. (i) Exciton migration between two dipyrrinato ligands coordinating to the same Zn ion is set to occur preferentially (path 1 in Fig. 6B); its probability is allowed to be greater than those for other processes. This supposition is supported by our previous experimental finding that energy transfer is highly effective in mononuclear heteroleptic complexes (e.g., Mono-4 in Fig. 1E) (*40*), presumably because of the direct contact of the molecular orbitals. (ii) A simplified Förster energy transfer scheme is used for other distant migrations (paths 2 to 4 in Fig. 6B). The transition moment of a dipyrrinato ligand is oriented at the molecular long axis (*48*, *49*). Our previous single-crystal x-ray structure analyses confirmed that the two dipyrrinate units in L1 or L3 are parallel to each other because of the bulky durene linker, and that the tetrahedral coordination sphere of the zinc center lets L1 and/or L3 arrange alternatively in a perpendicular fashion (*38*). The absorption spectra of the copolymer are consistent with those of its constitutive mononuclear complexes (fig. S17); therefore, ground-state interaction among the dipyrrinate units such as π-conjugation is trivial. In this situation, exciton transfer probabilities between dipyrrinato ligands perpendicular to each other are set to zero (path 3), whereas those between parallel ones have non-zero values with a distance decay (paths 2 and 4). Considering simplification and the distance decay effect, exciton transfer processes that are more distant than those shown in Fig. 6B are ignored. (iii) Among the four types of migration ($D_{L1}\rightarrow D_{L1}$, $D_{L3}\rightarrow D_{L3}$, $D_{L1}\rightarrow D_{L3}$, and $D_{L3}\rightarrow D_{L1}$), that for $D_{L1}\rightarrow D_{L3}$ is ignored because there is a negligible spectral overlap between PL from the former and absorption by the latter, and the excitation energy gap (0.3 eV) is greater than the thermal energy at room temperature (fig. S5). The numerical simulation is conducted as follows. One of the dipyrrinato ligands in the virtual strand is randomly chosen to be photoexcited with respect to the photoexcitation wavelength (i.e., D_{L1} for 550 nm; D_{L3} for 490 nm). Here, we define variable *N* as the number of exciton hops; after the *N*th hop, the exciton was consumed as PL or nonradiative decay with a certain

probability depending on the dipyrrinate site. Series of virtual wire generation, exciton generation and hopping, and exciton decay processes were repeated 100,000 times, and the average ϕ_{PL} is plotted with respect to x in Fig. 6 (C and D). For 550-nm excitation, the simulated plot is consistent with the experimental one and N is irrelevant to the simulation result (Fig. 6C). In sharp contrast, N plays a vital role in the reproduction of the plot for 490-nm excitation (Fig. 6D). The distinctive bell curve emerges as N increases, and similarity to the experimental result is found with $N \geq 70$. The PL lifetime spans 1.61 to 2.89 ns (table S2); therefore, the exciton hopping frequency is calculated to be at least 24 to 43 ns^{-1}, which is consistent with those for precedential pigment multiads (*50*, *51*). In summary of this section, the numerical simulation accounts for the PL enhancement in random copolymers Co-1-*k*, and the existence of fast intrawire exciton migration is also deduced.

DISCUSSION

We synthesized a series of 1D coordination random copolymers featuring the bis(dipyrrinato)zinc(II) complex motif by simply mixing two types of bridging dipyrrin proligand and zinc acetate under ambient conditions. The coordination copolymers were exfoliated into single strands by sonication in organic media and were characterized by XPS and UV/vis spectroscopy. The single strands had topographical heights intermediate between those of the corresponding homopolymers, and the height of the copolymers increased as the proportion of the bulky bridging dipyrrinato ligand increased. Spectroscopic studies for the exfoliated copolymers revealed intrawire exciton accumulation from the plain dipyrrinato ligand to the π-extended dipyrrinato ligand, reflecting their copolymer configuration. The heterostructure also enhanced the PL quantum yield of the copolymer nanowire, being consistent with our unique knowledge on mononuclear dipyrrinato-zinc(II) complexes. The PL enhancement was elucidated by a numerical simulation relying on a restricted random walk model, which also suggested the existence of fast intrawire exciton migration. The characteristic structural aspect of the present coordination nanowire—random copolymer composition and rigid, steric, and orthogonal 1D framework—realizes the abovementioned achievements. There is room yet to be investigated further, such as the deviation in the wire length, elucidation of the strand height distribution, and possibility of reaggregation after exfoliation. Nonetheless, the present work is conducted with unique concepts and approaches, contributing new strategies and knowledge in fundamental polymer and nanoscience, simultaneously demonstrating the potential utility of the present coordination polymers as photofunctional nanomaterials such as photonic wires.

MATERIALS AND METHODS

General experimental procedures

All chemicals were purchased from Tokyo Chemical Industry Co. Ltd., Kanto Chemical Co., or Wako Pure Chemical Industries Ltd., unless otherwise stated. They were used without further purification. HOPG was purchased from Alliance Biosystems Inc. (grade SPI-1, 10 mm × 10 mm × 2 mm) and was cleaved with adhesive tape just before use. Transparent SnO_2 electrodes (on indium tin oxide–coated glass, 5 ohms sq^{-1}) were purchased from Geomatec Co. Ltd. They were sonicated in acetone (10 min) and nonionic detergent in water (30 min × 2). Then, the substrates were washed with water until the bubble of the detergent disappeared and sonicated in water (10 min). The cleaned substrates were stored in water and dried by nitrogen flow just before use. The bridging proligands (H_2L1 and H_2L3) and the homoleptic nanowire (Homo-1) were synthesized according to the previously described methods (*38*, *43*). AFM was performed using an Agilent Technologies 5500 scanning probe microscope under an ambient condition. AFM was performed in high-amplitude mode (tapping mode), with a silicon cantilever Nano World NCH probe. Height profiles were measured in flat regions; data points with heights of >2.9 and <0.4 nm were excluded; we regarded them as irrelevant noise data. UV/vis spectra were recorded on a JASCO V-570 spectrometer. Fluorescence spectra were collected with a Hitachi F-4500 spectrometer. Absolute photoluminescent quantum yields were measured with a Hamamatsu Photonics C9920-02G instrument. Fluorescence lifetime measurements were conducted using a Hamamatsu Photonics Quantaurus-Tau C11367-02 instrument. ^{1}H and ^{13}C nuclear magnetic resonance (NMR) data were collected in $CDCl_3$ and recorded on a Bruker US500 spectrometer. Tetramethylsilane [δ_H = 0.00 parts per million (ppm)] was used as an internal standard for the ^{1}H NMR spectra, and $CDCl_3$ (δ_C = 77.00 ppm) was used as an internal standard for the ^{13}C NMR spectra. High-resolution fast-atom bombardment mass spectroscopy (HR-FAB-MS) was performed on a JEOL JMS-700 MStation mass spectrometer. HR electrospray ionization time-of-flight MS (HR-ESI-TOF-MS) was performed on a Waters LCT Premier XE spectrometer. Preparative gel permeation chromatography (GPC) was performed using LC-918 with JAIGEL 1H and 2H column (Japan Analytical Industry) using chloroform as the mobile phase.

Synthesis of heteroleptic bis(dipyrrinato)zinc(II) coordination copolymers, Co-1-*k*

A methanol solution (5 ml) of zinc(II) acetate (5 μmol) was added to a dichloromethane solution (10 ml) of H_2L1 and H_2L3 (the amounts of the ligands are listed in Fig. 1C). After several days, powdery solid was formed in the reaction mixture, which was collected by filtration, washed with methanol and dichloromethane, and then dried to obtain Co-1-*k*.

Synthesis of 5,5′-(2,3,5,6-tetramethyl-1,4-phenylene)bis((3,5-dimethyl-4-(2-(4-methoxyphenyl)ethynyl)-2*H*-pyrrol-2-ylidene)methylene))bis(2,4-dimethyl-3-(2-(4-methoxyphenyl)ethynyl)-1*H*-pyrrole), H_2L2

Under a nitrogen atmosphere, a mixture of 5,5′-(2,3,5,6-tetramethyl-1,4-phenylene)bis((3,5-dimethyl-4-iodo-2*H*-pyrrol-2-ylidene)methylene))bis(2,4-dimethyl-3-iodo-1*H*-pyrrole) (400.5 mg, 0.387 mmol), $Pd(PPh_3)_2Cl_2$ (13.8 mg, 0.020 mmol), CuI (3.8 mg, 0.020 mmol), and 1-ethynyl-4-methoxybenzene (338.8 mg, 2.56 mmol) in tetrahydrofuran (10 ml) and triethylamine (4 ml) was heated at 70°C for 4 hours. After evaporation of the solvent, the residue was purified by alumina column chromatography (eluent:hexane/dichloromethane = 2:1, then the ratio of dichloromethane was increased gradually up to 1:2). The red band was collected and evaporated, and the resultant residue was reprecipitated from dichloromethane and methanol to give H_2L2 as a red solid (90 mg, 22%). ^{1}H NMR (500 MHz, $CDCl_3$): δ = 7.43 (d, 8H, J = 8.8 Hz), 6.85 (d, 8H, J = 9.1 Hz), 3.82 (s, 12H), 2.50 (s, 12H), 2.15 (s, 12H), 1.60 (s, 12H); ^{13}C NMR (125 MHz, $CDCl_3$): δ = 159.29, 153.50, 140.58, 139.55, 136.15, 133.33, 132.98, 132.75, 132.66, 116.18, 113.97, 95.50, 82.05, 55.32, 17.21, 15.18, 14.50; HR-ESI-TOF-MS [mass/charge ratio (*m/z*)]: $[M + H]^+$, calculated for $C_{72}H_{67}N_4O_4^+$, 1051.5162; found, 1051.5095.

Synthesis of homoleptic bis(dipyrrinato)zinc(II) complex homopolymer, Homo-2

A methanol solution (2.5 ml) of zinc(II) acetate (0.46 mg, 2.5 μmol) was added to a dichloromethane solution (5 ml) of H_2L2 (2.08 mg, 2.0 μmol), and the mixture was stored in the dark. After 4 days, red powdery solid was formed in the reaction mixture, which was collected by filtration, washed with methanol and dichloromethane, and then dried to obtain Homo-2.

Synthesis of heteroleptic bis(dipyrrinato)zinc(II) coordination copolymers, Co-2-*k*

A methanol solution (5 ml) of zinc(II) acetate (5 μmol) was added to a dichloromethane solution (10 ml) of H_2L2 and H_2L3 (the amounts of the ligands are listed in Fig. 1D). After several days, powdery solid was formed in the reaction mixture, which was collected by filtration, washed with methanol and dichloromethane, and then dried to obtain Co-2-*k*.

Synthesis of homoleptic bis(dipyrrinato)zinc(II) complex homopolymer, Homo-3

A methanol solution (5 ml) of zinc(II) acetate (0.92 mg, 5.0 μmol) was added to a dichloromethane solution (10 ml) of H_2L3 (1.87 mg, 3.9 μmol), and the reaction mixture was stored in the dark. After 4 days, orange powdery solid was formed in the reaction mixture, which was collected by filtration, washed with methanol and dichloromethane, and then dried to obtain Homo-3.

Synthesis of 2-((3,5-dimethyl-4-(2-(4-methoxyphenyl)ethynyl)-2*H*-pyrrol-2-ylidene)(2,6-dimethylphenyl)methyl)-3,5-dimethyl-4-(2-(4-methoxyphenyl)ethynyl)-1*H*-pyrrole, HL4

Under a nitrogen atmosphere, a mixture of 2-((2,6-dimethylphenyl)(4-iodo-3,5-dimethyl-2*H*-pyrrol-2-ylidene)methyl)-4-iodo-3,5-dimethyl-1*H*-pyrrole (600.5 mg, 1.08 mmol), $Pd(PPh_3)_2Cl_2$ (36.62 mg, 0.052 mmol), CuI (10.4 mg, 0.055 mmol), and 1-ethynyl-4-methoxybenzene (395.3 mg, 2.99 mmol) in triethylamine (50 ml) was heated at 70°C and stirred at room temperature overnight. After evaporation of the solvent, the residue was purified by alumina column chromatography (eluent: hexane, then hexane/dichloromethane = 1:1). The red band was collected and evaporated, and the residue was reprecipitated from dichloromethane and hexane to give HL4 as a red solid (381.2 mg, 62%). ^{1}H NMR (500 MHz, CDCl3): δ = 7.38 (d, 8H, *J* = 8.8 Hz), 7.23 (dd, 1H, *J* = 7.6, 7.6 Hz), 7.11 (d, 2H, *J* = 7.6 Hz), 6.84 (d, 4H, *J* = 9.1 Hz), 3.81 (s, 6H), 2.49 (s, 6H), 2.13 (s, 6H), 1.41 (s, 6H); ^{13}C NMR (125 MHz, $CDCl_3$): δ = 159.24, 153.55, 140.76, 138.07, 136.31, 135.91, 135.37, 132.61, 128.42, 127.96, 116.22, 114.15, 113.94, 95.51, 82.12, 55.30, 19.60, 15.18, 12.39; HR-FAB-MS (*m/z*): $[M]^+$, calculated for $C_{39}H_{36}N_2O_2^+$, 564.2777; found, 564.2755.

Synthesis of mononuclear heteroleptic bis(dipyrrinato)zinc(II) complex, Mono-5

A methanol solution (6 ml) of zinc(II) acetate (73.9 mg, 0.40 mmol) was added to a dichloromethane solution (40 ml) of 2-((2,6-dimethylphenyl)(5-methyl-2*H*-pyrrol-2-ylidene)methyl)-5-methyl-1*H*-pyrrole (166.4 mg, 0.60 mmol) and HL4 (113.1 mg, 0.20 mmol). After stirring the reaction mixture overnight, the solvent was evaporated and the residue was purified by GPC to give Mono-5 as a red brown solid (36.6 mg, 20.2%). ^{1}H NMR (500 MHz, CD_2Cl_2): δ = 7.33 (d, 4H, *J* = 8.8 Hz), 7.30 (dd, 1H, *J* = 7.2, 7.2 Hz), 7.25 (dd, 1H, *J* = 7.6, 7.6 Hz), 7.19 (d, 2H, *J* = 7.2 Hz), 7.13 (d, 2H, *J* = 7.9 Hz), 6.82 (d, 4H, *J* = 9.1 Hz), 6.40 (d, 2H, *J* = 4.1 Hz), 6.17 (d, 2H, *J* = 4.1 Hz), 3.79 (s, 6H), 2.18 (s, 6H), 2.18 (s, 6H), 2.17 (s, 6H), 2.14 (s, 6H), 1.44 (s, 6H); ^{13}C NMR (125 MHz, $CDCl_3$): δ = 159.24, 153.55, 140.76, 138.07, 136.31, 135.91, 135.37, 132.61, 128.42, 127.96, 116.22, 114.15, 113.94, 95.51, 82.12, 55.30, 19.60, 15.18, 12.39; HR-ESI-TOF-MS (*m/z*): $[M]^+$, calculated for $C_{58}H_{54}N_4O_2Zn^+$, 902.3522; found, 902.3538.

Single-crystal x-ray diffraction analysis

Single crystals of dipyrrin proligands H_2L3·2HBr and H_2L3′·2HBr·$(solvent)_n$ were prepared as follows. Dipyrrin proligand H_2L3 (0.84 mmol, 1 eq) was dissolved in methanol (50 ml) by adding 48% HBr aq. (3.7 mmol, 4.4 eq). Then, diethyl ether (200 ml) was poured into the solution, giving a microcrystalline powder of H_2L3·2HBr. Its single crystals suitable for x-ray diffraction analysis were grown by vapor diffusion of diethyl ether into an ethanol solution of H_2L3·2HBr. A similar method was applied to H_2L3′, and single crystals of H_2L3′·2HBr·$(solvent)_n$ were obtained by vapor diffusion of diethyl ether into a methanol solution of H_2L3′·2HBr. Diffraction data were collected at 93 K on a Rigaku Saturn 724 (VariMax dual) diffractometer with multilayer mirror monochromated MoKα radiation using Crystal Clear (Rigaku). The structures were solved by means of the direct method using SIR92 and refined by the full-matrix least squares using SHELXL-97. Because of severe disorder, solvent molecules in the crystal structure of H_2L3′·2HBr·$(solvent)_n$ were removed using the SQUEEZE routine of the PLATON software when necessary, after which the structures were refined again using the data generated. CCDC 1867482 [for H_2L3′·2HBr·$(solvent)_n$] and 1867483 (for H_2L3·2HBr) contain the supplementary crystallographic data for this paper. These data may be obtained free of charge from The Cambridge Crystallographic Data Centre via www.ccdc.cam.ac.uk/data_request/cif.

UV/vis absorption in solution

A dispersion of each of the prepared polymers in toluene was subjected to UV/vis spectroscopy. The baselines of the UV/vis spectra were corrected to exclude the effect of light scattering.

Mole fraction of L1 in Co-1-*k*

The mole fraction of L1 in Co-1-*k*, *x*, was determined from the UV/vis absorption spectra in toluene. Co-1-*k* has two main absorption peaks at 490 and 550 nm, which are derived from L3 and L1, respectively. We assumed that the influence of L3 is negligible in the absorption at 550 nm, and that of L1 is sufficiently small at the 490-nm absorption. Dividing the absorbance at 550 nm by the molar extinction coefficient of corresponding mononuclear heteroleptic complex Mono-4 at 550 nm (1.0×10^5 M^{-1} cm^{-1}) gave q_1, the quantity of L1. That of L3, q_3, can be also obtained in the same manner using the molar extinction coefficient of Mono-4 at 490 nm (1.1×10^5 M^{-1} cm^{-1}). *x* was calculated using the following equation

$$x = q_1/(q_1 + q_3) \quad (4)$$

Figure 2F shows the relationship between *x* and the mixing ratio of H_2L1 to (H_2L1 + H_2L3) (*r*) in the wire formation reaction. The slope of the plot was calculated to be 0.84.

Mole fraction of L2 in Co-2-*k*

The mole fraction of L2 in Co-2-*k*, *x*′, was determined using the same method as that for *x*, except that Mono-5 was used as a referential

mononuclear heteroleptic complex showing 1.0×10^5 and 1.3×10^5 M^{-1} cm^{-1} for the molar extinction coefficient at 550 and 490 nm, respectively. Figure S6C shows the relationship between x' and r'. The slope of the plot was calculated to be 0.97.

Photovoltaic conversion

A dichloromethane dispersion of Co-1-6, Homo-1, or Homo-3 was dropcast on a transparent SnO_2 electrode so that the polymer was deposited in the range of a 5-mmØ circle. The coordination polymer deposited on the SnO_2 electrode was always subjected to UV/vis spectroscopy before the photovoltaic conversion experiment. The baseline of the UV/vis spectrum was corrected to exclude the effect of light scattering caused by the coordination polymer film. The modified SnO_2 electrode was used as a working electrode (photoanode). A homemade Ag^+/Ag reference electrode (0.01 M $AgClO_4$ in 0.1 M Bu_4NClO_4/acetonitrile for Co-1-6 and Homo-3) and a Pt wire counter electrode were implemented to establish a three-electrode system. The three electrodes were assembled into a photoelectrochemical cell in the same way as in the previous work (*38*). The cell was filled with an acetonitrile solution of Bu_4NClO_4 (0.1 M, as a supporting electrolyte) containing triethanolamine (TEOA; 0.05 M, as a sacrificial donor reagent). As for Homo-1, aqueous sodium sulfate (0.1 M) containing 0.03 M TEOA as an electrolyte solution and an Ag/AgCl reference electrode were used because of good dispersibility of Homo-1 in acetonitrile. The photoelectrochemical cell was sealed and deoxygenized by Ar bubbling for 5 min before the measurement. Monochromatic light for the acquisition of the action spectrum shown in fig. S7 (C to E) (450 to 600 nm in every 10 nm) was extracted from Xe lamp (MAX-302, Asahi Spectra Co. Ltd.), the photon flux of which was monochromated by a monochromator (CT-10, JASCO Corporation). For the photocurrent response shown in fig. S7B, monochromic light was provided by a Xe lamp equipped with a band-pass filter (500 nm). The active area of the electrode was fixed at 0.264 cm^2, which was determined by a fluorocarbon rubber O-ring. The electrode potential was controlled using an electrochemical analyzer (ALS-750A, BAS Inc.). The potential of the photoanode was fixed at near the open circuit potential such that a negligible dark current was observed. The photocurrent was also collected through the electrochemical analyzer.

DFT calculation

The geometrical optimization and estimation of the electronic structure for Mono-1, Mono-3′, Mono-3′′ (fig. S11D), and Mono-4 were carried out using the Gaussian 09 program (version 9.6). The structure was optimized without any symmetry constraint. The 6-31G(d) basis set and B3LYP hybrid exchange-correlation functional were used. Visualization of the molecular orbitals was performed using GaussView 5.0.8 software.

Inductively coupled plasma atomic emission spectrometry

Samples for ICP-AES study were prepared using an acid digestion method. Concentrated sulfuric acid (1 ml) was added to a weighed sample in a sample tube, which was then placed in an aluminum heating block at 200°C. Subsequently, 3 ml of concentrated nitric acid was added and the mixture was kept at 200°C until the sample was digested completely. The resulting solution was transferred in a 50-ml volumetric flask and diluted with water. Diluted zinc standard solutions with 2% (v/v) sulfuric acid were also prepared for calibration. ICP-AES measurements were performed on Shimadzu ICPS-7510 equipment.

Numerical simulation for the PL quantum yield of the coordination copolymers

The essence of the simulation is given in the Numerical simulation for the PL property section and Fig. 6; here, complementary information is described. We assumed that the two dipyrrinato ligands at the termini of the strand were adjacent to each other for the simplicity of the simulation. The probability of exciton transfer between two dipyrrinato ligands (p) was defined as $p = \alpha\beta$, where α reflects the energy migration type (paths 1 to 4 in Fig. 6B) and β is determined by the combination of the exciton donor and acceptor dipyrrinato ligands: α (path 1) = 0.75, α (path 2) = 0.2, α (path 3) = 0, α (path 4) = 0.05, β ($D_{L1} \rightarrow D_{L1}$) = β ($D_{L3} \rightarrow D_{L1}$) = β ($D_{L3} \rightarrow D_{L3}$) = 1, and β ($D_{L1} \rightarrow D_{L3}$) = 0. The α values for paths 2 and 4 correspond to a distance decay with a Förster radius of 1.5 nm. The probabilities (ϕ) of PL emission after the N^{th} exciton hop were set as follows: ϕ ($D_{Homo\text{-}L3}$) = 0.10, ϕ ($D_{Homo\text{-}L1}$) = 0.03, and ϕ ($D_{Hetero\text{-}L3}$) = ϕ ($D_{Hetero\text{-}L1}$) = 0.40. The ϕ values for $D_{Homo\text{-}L3}$ and $D_{Homo\text{-}L1}$ were determined from ϕ_{PL} of Homo-3 and Homo-1, while those of $D_{Hetero\text{-}L3}$ and $D_{Hetero\text{-}L1}$ were assumed from the fact that a mononuclear heteroleptic bis(dipyrrinato)zinc(II) complex showed quantitative intramolecular, interligand exciton transfer and that it showed higher PL quantum yield than corresponding homoleptic complexes (*40*, *44*). A homemade program was implemented to conduct the numerical simulation.

SUPPLEMENTARY MATERIALS

Supplementary material for this article is available at http://advances.sciencemag.org/cgi/content/full/5/1/eaau0637/DC1

Fig. S1. Oak Ridge thermal ellipsoid plot drawings of $H_2L3{\cdot}2HBr$ and $H_2L3'{\cdot}2HBr{\cdot}(solvent)_n$ with a thermal ellipsoid set at the 50% probability level.
Fig. S2. XPS for proligands and coordination polymers.
Fig. S3. Quantification of the elemental ratio from XPS.
Fig. S4. Elemental abundances in Co-1-*k* and Homo-1 determined by elemental and ICP-AES analysis.
Fig. S5. PL enhancement mechanism for a heteroleptic complex.
Fig. S6. UV/vis spectroscopy for Co-2-*k* in toluene.
Fig. S7. Photovoltaic conversion of Co-1-6, Homo-3, and Homo-1.
Fig. S8. Three-electrode electrochemical cell used for the photoelectric conversion.
Fig. S9. AFM images of Co-1-3 on other substrates.
Fig. S10. AFM for Homo-1.
Fig. S11. AFM for Homo-3′.
Fig. S12. Gaussian fitting of AFM height histograms of Co-1-*k*, Homo-1, and Homo-3′.
Fig. S13. PL lifetimes (τ_{PL}) in toluene.
Fig. S14. PL of Co-2-*k* in toluene.
Fig. S15. PL quantum yield dependence on x' in toluene.
Fig. S16. Calculated ϕ_{PL} dependence on x.
Fig. S17. UV/vis absorption spectroscopy for copolymers and corresponding mononuclear complexes in toluene.
Table S1. Crystallographic data.
Table S2. PL properties of Co-1-*k*, Homo-1, and Homo-3 in toluene.

REFERENCES AND NOTES

1. G. Klärner, M. H. Davey, W.-D. Chen, J. C. Scott, R. D. Miller, Colorfast blue-light-emitting random copolymers derived from di-*n*-hexylfluorene and anthracene. *Adv. Mater.* **10**, 993–997 (1998).
2. P. T. Furuta, L. Deng, S. Garon, M. E. Thompson, J. M. J. Fréchet, Platinum-functionalized random copolymers for use in solution-processible, efficient, near-white organic light-emitting diodes. *J. Am. Chem. Soc.* **126**, 15388–15389 (2004).
3. J.-M. Jiang, H.-C. Chen, H.-K. Lin, C.-M. Yu, S.-C. Lan, C.-M. Liu, K.-H. Wei, Conjugated random copolymers of benzodithiophene–benzooxadiazole–diketopyrrolopyrrole with full visible light absorption for bulk heterojunction solar cells. *Polym. Chem.* **4**, 5321–5328 (2013).
4. S. Kim, H. S. Wang, Y. Choe, S.-H. Choi, J. Bang, Controlling the microdomain orientation in block copolymer thin films via cross-linkable random copolymer neutral layer. *Polym. J.* **48**, 333–340 (2016).

5. M. Onoda, T. Ueki, R. Tamate, M. Shibayama, R. Yoshida, Amoeba-like self-oscillating polymeric fluids with autonomous sol-gel transition. *Nat. Commun.* **8**, 15862 (2017).
6. K. Kataoka, A. Harada, Y. Nagasaki, Block copolymer micelles for drug delivery: Design, characterization and biological significance. *Adv. Drug Deliv. Rev.* **64**, 37–48 (2012).
7. M. Lazzari, M. A. López-Quintela, Block copolymers as a tool for nanomaterial fabrication. *Adv. Mater.* **15**, 1583–1594 (2003).
8. A.-V. Ruzette, L. Leibler, Block copolymers in tomorrow's plastics. *Nat. Mater.* **4**, 19–31 (2005).
9. X. Wang, G. Guerin, H. Wang, Y. Wang, I. Manners, M. A. Winnik, Cylindrical block copolymer micelles and co-micelles of controlled length and architecture. *Science* **317**, 644–647 (2007).
10. H. Qiu, Z. M. Hudson, M. A. Winnik, I. Manners, Multidimensional hierarchical self-assembly of amphiphilic cylindrical block comicelles. *Science* **347**, 1329–1332 (2015).
11. X. Li, Y. Gao, C. E. Boott, M. A. Winnik, I. Manners, Non-covalent synthesis of supermicelles with complex architectures using spatially confined hydrogen-bonding interactions. *Nat. Commun.* **6**, 8127 (2015).
12. H. Bin, L. Gao, Z.-G. Zhang, Y. Yang, Y. Zhang, C. Zhang, S. Chen, L. Xue, C. Yang, M. Xiao, Y. Li, 11.4% Efficiency non-fullerene polymer solar cells with trialkylsilyl substituted 2D-conjugated polymer as donor. *Nat. Commun.* **7**, 13651 (2016).
13. C. Li, H. Yan, L.-X. Zhao, G.-F. Zhang, Z. Hu, Z.-L. Huang, M.-Q. Zhu, A trident dithienylethene-perylenemonoimide dyad with super fluorescence switching speed and ratio. *Nat. Commun.* **5**, 5709 (2014).
14. P. Roy, A. Jha, V. B. Yasarapudi, T. Ram, B. Puttaraju, S. Patil, J. Dasgupta, Ultrafast bridge planarization in donor-π-acceptor copolymers drives intramolecular charge transfer. *Nat. Commun.* **8**, 1716 (2017).
15. J. S. Ha, K. H. Kim, D. H. Choi, 2,5-Bis(2-octyldodecyl)pyrrolo[3,4-*c*]pyrrole-1,4-(2*H*,5*H*)-dione-based donor–acceptor alternating copolymer bearing 5,5′-Di(thiophen-2-yl)-2,2′-biselenophene exhibiting 1.5 $cm^2 V^{-1} s^{-1}$ hole mobility in thin-film transistors. *J. Am. Chem. Soc.* **133**, 10364–10367 (2011).
16. J. Lee, S. B. Jo, M. Kim, H. G. Kim, J. Shin, H. Kim, K. Cho, Donor–acceptor alternating copolymer nanowires for highly efficient organic solar cells. *Adv. Mater.* **26**, 6706–6714 (2014).
17. F. Zhang, W. Mammo, L. M. Andersson, S. Admassie, M. R. Andersson, O. Inganäs, Low-bandgap alternating fluorene copolymer/methanofullerene heterojunctions in efficient near-infrared polymer solar cells. *Adv. Mater.* **18**, 2169–2173 (2006).
18. D. Di Nuzzo, C. Fontanesi, R. Jones, S. Allard, I. Dumsch, U. Scherf, E. von Hauff, S. Schmacher, E. Da Como, How intermolecular geometrical disorder affects the molecular doping of donor–acceptor copolymers. *Nat. Commun.* **6**, 6460 (2015).
19. S. Mochizuki, N. Ogiwara, M. Takayanagi, M. Nagaoka, S. Kitagawa, T. Uemura, Sequence-regulated copolymerization based on periodic covalent positioning of monomers along one-dimensional nanochannels. *Nat. Commun.* **9**, 329 (2018).
20. A. Kermagoret, A. Debuigne, C. Jérôme, C. Detrembleur, Precision design of ethylene- and polar-monomer-based copolymers by organometallic-mediated radical polymerization. *Nat. Chem.* **6**, 179–187 (2014).
21. J. C. Barnes, D. J. C. Ehrlich, A. X. Gao, F. A. Leibfarth, Y. Jiang, E. Zhou, T. F. Jamison, J. A. Johnson, Iterative exponential growth of stereo- and sequence-controlled polymers. *Nat. Chem.* **7**, 810–815 (2015).
22. D. J. van Dijken, P. Štacko, M. C. A. Stuart, W. R. Browne, B. L. Feringa, Chirality controlled responsive self-assembled nanotubes in water. *Chem. Sci.* **8**, 1783–1789 (2017).
23. P. Besenius, Controlling supramolecular polymerization through multicomponent self-assembly. *J. Polym. Sci. A Polym. Chem.* **55**, 34–78 (2017).
24. S. K. Yang, A. V. Ambade, M. Weck, Supramolecular alternating block copolymers via metal coordination. *Chemistry* **15**, 6605–6611 (2009).
25. M. N. Higley, J. M. Pollino, E. Hollembeak, M. Weck, A modular approach toward block copolymers. *Chemistry* **11**, 2946–2953 (2006).
26. J. M. Pollino, L. P. Stubbs, M. Weck, One-step multifunctionalization of random copolymers via self-assembly. *J. Am. Chem. Soc.* **126**, 563–567 (2004).
27. T. Hirao, H. Kudo, T. Amimoto, T. Haino, Sequence-controlled supramolecular terpolymerization directed by specific molecular recognitions. *Nat. Commun.* **8**, 634 (2017).
28. A. Das, G. Vantomme, A. J. Markvoort, H. M. M. ten Eikelder, M. Garcia-Iglesias, A. R. A. Palmans, E. W. Meijer, Supramolecular copolymers: Structure and composition revealed by theoretical modeling. *J. Am. Chem. Soc.* **139**, 7036–7044 (2017).
29. L. Brunsveld, B. J. B. Folmer, E. W. Meijer, R. P. Sijbesma, Supramolecular polymers. *Chem. Rev.* **101**, 4071–4098 (2001).
30. L. Yang, X. Tan, Z. Wang, X. Zhang, Supramolecular polymers: Historical development, preparation, characterization, and functions. *Chem. Rev.* **115**, 7196–7239 (2015).
31. P. Ares, P. Amo-Ochoa, J. M. Soler, J. J. Palacios, J. Gómez-Herrero, F. Zamora, High electrical conductivity of single metal–organic chains. *Adv. Mater.* **30**, 1705645 (2018).
32. R. Mas-Ballesté, J. Gómez-Herrero, F. Zamora, One-dimensional coordination polymers on surfaces: Towards single molecule devices. *Chem. Soc. Rev.* **39**, 4220–4233 (2010).
33. M.-R. Azani, A. P. Paz, C. Hermosa, G. Givaja, J. Gómez-Herrero, R. Mas-Ballesté, F. Zamora, A. Rubio, The isolation of single MMX chains from solution: Unravelling the assembly-disassembly process. *Chemistry* **19**, 15518–15529 (2013).
34. H. Masai, J. Terao, S. Seki, S. Nakashima, M. Kiguchi, K. Okoshi, T. Fujihara, Y. Tsuji, Synthesis of one-dimensional metal-containing insulated molecular wire with versatile properties directed toward molecular electronics materials. *J. Am. Chem. Soc.* **136**, 1742–1745 (2014).
35. T. Ohshiro, Y. Umezawa, Complementary base-pair-facilitated electron tunneling for electrically pinpointing complementary nucleobases. *Proc. Natl. Acad. Sci. U.S.A.* **103**, 10–14 (2006).
36. H. Tanaka, T. Kawai, Partial sequencing of a single DNA molecule with a scanning tunnelling microscope. *Nat. Nanotechnol.* **4**, 518–522 (2009).
37. H. Tanaka, T. Kawai, Visualization of detailed structures within DNA. *Surf. Sci.* **539**, L531–L536 (2003).
38. R. Matsuoka, R. Toyoda, R. Sakamoto, M. Tsuchiya, K. Hoshiko, T. Nagayama, Y. Nonoguchi, K. Sugimoto, E. Nishibori, T. Kawai, H. Nishihara, Bis(dipyrrinato)metal(II) coordination polymers: Crystallization, exfoliation into single wires, and electric conversion ability. *Chem. Sci.* **6**, 2853–2858 (2015).
39. R. Aoki, R. Toyoda, J. F. Kögel, R. Sakamoto, J. Kumar, Y. Kitagawa, K. Harano, T. Kawai, H. Nishihara, Bis(dipyrrinato)zinc(II) complex chiroptical wires: Exfoliation into single strands and intensification of circularly polarized luminescence. *J. Am. Chem. Soc.* **139**, 16024–16027 (2017).
40. S. Kusaka, R. Sakamoto, Y. Kitagawa, M. Okumura, H. Nishihara, An extremely bright heteroleptic bis(dipyrrinato)zinc(II) complex. *Chemistry* **7**, 907–910 (2012).
41. R. Sakamoto, T. Iwashima, M. Tsuchiya, R. Toyoda, R. Matsuoka, J. F. Kögel, S. Kusaka, K. Hoshiko, T. Yagi, T. Nagayama, H. Nishihara, New aspects in bis and tris(dipyrrinato)metal complexes: Bright luminescence, self-assembled nanoarchitectures, and materials applications. *J. Mater. Chem. A* **3**, 15357–15371 (2015).
42. R. Toyoda, M. Tsuchiya, R. Sakamoto, R. Matsuoka, K.-H. Wu, Y. Hattori, H. Nishihara, Heteroleptic bis(dipyrrinato)copper(II) and nickel(II) complexes. *Dalton Trans.* **44**, 15103–15106 (2015).
43. M. Tsuchiya, R. Sakamoto, S. Kusaka, Y. Kitagawa, M. Okumura, H. Nishihara, Asymmetric dinuclear bis(dipyrrinato)zinc(II) complexes: Broad absorption and unidirectional quantitative exciton transmission. *Chem. Commun.* **50**, 5881–5883 (2014).
44. R. Sakamoto, T. Iwashima, J. F. Kögel, S. Kusaka, M. Tsuchiya, Y. Kitagawa, H. Nishihara, Dissymmetric bis(dipyrrinato)zinc(II) complexes: Rich variety and bright red to near-infrared luminescence with a large pseudo-stokes shift. *J. Am. Chem. Soc.* **138**, 5666–5677 (2016).
45. J. F. Kögel, S. Kusaka, R. Sakamoto, T. Iwashima, M. Tsuchiya, R. Toyoda, R. Matsuoka, T. Tsukamoto, J. Yuasa, Y. Kitagawa, T. Kawai, H. Nishihara, Heteroleptic [bis(oxazoline)](dipyrrinato)zinc(II) complexes: Bright and circularly polarized luminescence from an originally achiral dipyrrinato ligand. *Angew. Chem. Int. Ed. Engl.* **55**, 1377–1381 (2016).
46. R. Sakamoto, K. Hoshiko, Q. Liu, T. Yagi, T. Nagayama, S. Kusaka, M. Tsuchiya, Y. Kitagawa, W.-Y. Wong, H. Nishihara, A photofunctional bottom-up bis(dipyrrinato)zinc(II) complex nanosheet. *Nat. Commun.* **6**, 6713 (2015).
47. R. Sakamoto, T. Yagi, K. Hoshiko, S. Kusaka, R. Matsuoka, H. Maeda, Z. Liu, Q. Liu, W.-Y. Wong, H. Nishihara, Photofunctionality in porphyrin-hybridized bis(dipyrrinato)zinc(II) complex micro- and nanosheets. *Angew. Chem. Int. Ed. Engl.* **56**, 3526–3530 (2017).
48. S. G. Telfer, T. M. McLean, M. R. Waterland, Exciton coupling in coordination compounds. *Dalton Trans.* **40**, 3097–3108 (2011).
49. T. Bruhn, G. Pescitelli, S. Jurinovich, A. Schaumlöffel, F. Witterauf, J. Ahrens, M. Bröring, G. Bringmann, Axially chiral BODIPY DYEmers: An apparent exception to the exciton chirality rule. *Angew. Chem. Int. Ed. Engl.* **53**, 14592–14595 (2014).
50. H. Langhals, A. J. Esterbauer, A. Walter, E. Riedle, I. Pugliesi, Förster resonant energy transfer in orthogonally arranged chromophores. *J. Am. Chem. Soc.* **132**, 16777–16782 (2010).
51. F. Schweighöfer, L. Dworak, C. A. Hammer, H. Gustmann, M. Zastrow, K. Rück-Braun, J. Wachtveitl, Highly efficient modulation of FRET in an orthogonally arranged BODIPY–DTE dyad. *Sci. Rep.* **6**, 28638 (2016).

Acknowledgments

Funding: The present work was chiefly supported by JST-PRESTO "Hyper-nano-space design toward innovative functionality" to R.S. (JPMJCR15F2). We also acknowledge grants-in-aid from MEXT of Japan [nos. 17H05354 and 18K19094, area 2802 (Coordination Asymmetry)]. R.T., R.M., and M.T. thank JSPS Research Fellowships for Young Scientists. R.S. is grateful to Iketani Science and Technology Foundation, Kumagai Foundation for Science and Technology, Foundation for Interaction in Science and Technology, The Foundation for The Promotion of Ion Engineering, Foundation Advanced Technology Institute, Izumi Science and Technology Foundation, LIXIL JS Foundation, Tonen General Sekiyu R&D Encouragement and Assistance

Foundation, The Iwatani Naoji Foundation, Hitachi Metals · Materials Science Foundation, The Murata Science Foundation, Kato foundation for Promotion of Science, and Yashima Environment Technology Foundation for financial support. The authors acknowledge the Research Hub Advanced Nano Characterization (Graduate School of Engineering, The University of Tokyo) for the XPS and single-crystal XRD study. We acknowledge T. Yasukawa (The University of Tokyo) for the ICP-AES analysis. **Author contributions:** R.S. and R.T. initiated the present work, and R.S. and H.N. directed it. R.T. and M.T. conducted the synthesis of the ligands and the mononuclear complexes. R.T. performed the synthesis of coordination polymers Homo-1, Homo-2, Homo-3, Co-1-*k*, and Co-2-*k*; DFT calculations; and photophysical measurements. R.T. and R.M. performed AFM measurements. N.F. conducted numerical calculations. R.S. and R.T. wrote the manuscript, and the rest of the authors commented on it. **Competing interests:** The authors declare that they have no competing interests. **Data and materials availability:** All data needed to evaluate the conclusions in the paper are present in the paper and/or the Supplementary Materials. Additional data related to this paper may be requested from the authors.

Submitted 12 May 2018
Accepted 26 November 2018
Published 4 January 2019
10.1126/sciadv.aau0637

Citation: R. Toyoda, R. Sakamoto, N. Fukui, R. Matsuoka, M. Tsuchiya, H. Nishihara, A single-stranded coordination copolymer affords heterostructure observation and photoluminescence intensification. *Sci. Adv.* **5**, eaau0637 (2019).